Published in final edited form as:
Dev Cell. 2007 February ; 12(2): 221–234. doi:10.1016/j.devcel.2006.12.003.

BIM Regulates Apoptosis During Mammary Ductal Morphogenesis and its Absence Reveals Alternative Cell Death Mechanisms

Arnaud A. Mailleux[*], **Michael Overholtzer**[*,1], **Tobias Schmelzle**[*,1], **Philippe Bouillet**[†], **Andrs Strasser**[†], and **Joan S. Brugge**[*,§]

[*] *Department of Cell Biology, Harvard Medical School, Boston, MA 02115, USA*

[†] *The Walter and Eliza Hall Institute of Medical Research, Melbourne, Victoria 3050, Australia*

Summary

The adult virgin mammary gland is a highly organized tree-like structure formed by ducts with hollowed *lumen*. Although *lumen* formation during pubertal development appears to involve apoptosis, the molecular mechanisms that regulate this process are not known. Here we demonstrate that disruption of the BH3-only pro-apoptotic factor *Bim* in mice prevents induction of apoptosis in and clearing of the *lumen* in terminal end buds during puberty. However, cells that fill the presumptive luminal space are eventually cleared from the adjacent ducts by a caspase-independent death process. Within the filled $Bim^{-/-}$ ducts, epithelial cells are deprived of matrix attachment and undergo squamous differentiation prior to clearing. Similarly, we also detect squamous differentiation *in vitro* when immortalized mammary epithelial cells are detached from matrix. These data provide important mechanistic information on the processes involved in sculpting the mammary gland and demonstrate that BIM is a critical regulator of apoptosis *in vivo*.

Keywords

BH3-only BCL-2 protein; BIM; apoptosis; mammary gland development; terminal end bud; caspase-independent cell death; CICD; squamous transdifferentiation

Introduction

During embryogenesis and puberty, the mammary gland undergoes a morphogenetic program that leads to the development of a hollow ductal system terminating in alveolae. Mammary development during puberty is an excellent model to study the process of *lumen* formation *in vivo*. From four weeks to eight weeks after birth, the rudimentary mammary tree undergoes extensive expansion that results from proliferation and invasion at the leading front of the ductal outgrowths. The highly proliferative bulbous structures at the tips of these expanding outgrowths, referred to as terminal end buds (TEBs), develop in response to elevation in reproductive hormones. A luminal space forms behind the TEB during ductal expansion and

§To whom correspondence should be addressed. Phone: (617) 432-3974 Fax: (617) 432-3969 E-mail: E-mail: joan_brugge@hms.harvard.edu.

[1]These two authors contributed equally to this work.

this process is hypothesized to require clearance of an inner cell population by apoptosis (Humphreys et al., 1996).

The TEB is composed of two main cell populations, distinguishable by their morphology and expression of specific markers: the cap cells and the body cells (Daniel et al., 1995). The cap cells are located in the outer layer in contact with the stroma and are considered to be progenitors of the myoepithelial cells. The body cells, organized with six to ten cell layers within the TEB, are thought to be precursors for the luminal lineage. A rare scattered third population is occasionally observed in the TEB body which expresses cap/myoepithelial cell markers and is hypothesized to comprise cap cells left behind during the extensive TEB outgrowth (Williams and Daniel, 1983).

It was previously shown that apoptosis is detected in non-proliferating body cells of TEBs (Humphreys et al., 1996). The spatial and temporal pattern of apoptosis suggested that caspase-mediated apoptosis maintains the *lumen* within the expanding duct. In addition, mosaic over-expression of *Bcl-2* was found to partially suppress body cell apoptosis and disrupt TEB structure. However, *lumen* formation was not inhibited and mature virgin mammary glands developed normally in this transgenic model (Humphreys et al., 1996). Thus, the mosaic over-expression of *Bcl-2* precluded evaluation of the consequences of inhibition of apoptosis in this model. While apoptosis is detected in TEBs of the developing glands, the mechanisms underlying *lumen* formation and the mediators of this process are not known. Elucidation of this apoptotic program is critical not only to understanding mammary gland development but also tumorigenesis, as repopulation of the luminal space with cancer cells is a hallmark of early breast tumors.

One potential mechanism for the regulation of luminal apoptosis has been proposed from studies utilizing a 3-dimensional (3D) *in vitro* model of mammary acini. Human MCF-10A mammary epithelial cells (MEC) grown in 3D cultures form acini-like structures with a hollow *lumen* that clears by an apoptotic program. Because the inner acinar cells that lack attachment to extracellular matrix (ECM) undergo apoptosis, it has been proposed that matrix deprivation, at least in part, contributes to the induction of apoptosis by a process analogous to anoikis. This term refers to cell death programs caused by matrix detachment (Frisch and Francis, 1994). In the 3D model, caspase activation is regulated by induction of the pro-apoptotic factor BIM (Reginato et al., 2005). BIM is a BH3-only member of the pro-apoptotic Bcl-2 intracellular protein family, which also includes Bmf, Bik, Bad, Bid, Puma, Noxa and Hrk (Huang and Strasser, 2000). During apoptosis, these proteins activate cytochrome *c* release and subsequent caspase activation by binding and inhibiting anti-apoptotic Bcl-2 family member proteins or triggering Bax oligomerization (Huang and Strasser, 2000). In the MCF-10A 3D model, *BIM* expression correlates temporally with *lumen* formation, and inhibition of *BIM* expression by small interfering RNA (siRNA) significantly delays apoptotic cell death of the central cell cluster (Reginato et al., 2005). Inhibition of *BIM* expression by siRNA also decreased apoptosis of MCF-10A cells during anoikis (Reginato et al., 2003). These data demonstrate that *lumen* formation in mammary acini and apoptosis during anoikis are dependent on the induction of BIM. However, whether BIM is a regulator of caspase activation and *lumen* formation in the mammary gland *in vivo* is not known. Furthermore, other mechanisms of anoikis in mouse MEC lines have been reported that apparently do not involve regulation by BIM (Wang et al., 2004). It is not known which of these *in vitro* models might be most representative of luminal death in the mammary gland *in vivo*.

To investigate the molecular mechanisms underlying apoptosis in mammary gland morphogenesis, we have examined the role of BIM-mediated cell death utilizing $Bim^{-/-}$ mice (Bouillet et al., 2001). Our results indicate that *Bim* is expressed constitutively in the mammary epithelium from the earliest stage of embryonic development. Mammary epithelial cells

lacking *Bim* were deficient for apoptosis induction in the TEB and ducts at five weeks and this was associated with an absence of *lumen* formation. Surprisingly, ducts in the $Bim^{-/-}$ mouse showed signs of caspase-independent death and squamous differentiation, and by eight weeks the luminal spaces in these ducts had hollowed. These data demonstrate that BIM is required for caspase-dependent cell death in the mammary gland and that in the absence of primary death mechanisms, such as apoptosis, alternative clearance mechanisms contribute to proper *lumen* formation in the mammary gland *in vivo*.

Results

Bim is widely expressed during mammary gland development in the mouse

Bim expression was analyzed during mouse mammary development by X-Gal whole mount staining of heterozygous $Bim^{+/LacZ}$ embryos (Bouillet et al., 2001). *Bim* expression was detected in mammary buds that arise from the epidermal embryo flank at E12.5 (Figure 1A). Thereafter, *Bim* expression was maintained in mammary epithelium throughout embryonic mammary gland development (Figure 1A–C). *Bim* was also detected in the epithelial placode of primordial hair follicles at E14.5 (β-galactosidase activity), which like the mammary buds are appendages, derived from the ectoderm (Figure 1B). At E18.5, *Bim* expression was detected in the mammary gland as well as in the fat pad precursor (Figure 1C). Following this period, *Bim* expression became restricted to the mammary epithelium (ducts and TEBs) during pubertal development (Figure 1D–E). Paraffin sections of the X-Gal stained mammary glands at five weeks showed that *Bim* is expressed in both mammary luminal and myoepithelial cells (data not shown). A previous report had shown that *Bim* mRNA was detected in the mature gland by *in situ* hybridization (O'Reilly et al., 2000). Here, we show that BIM is also expressed at the protein level in mammary TEBs (Figure 1F–G) and ducts (Figure 1H). As a control, we detected no BIM expression in $Bim^{-/-}$ mammary tissue sections using the same antibody (data not shown).

Loss of *Bim* triggers a transient luminal filling in the TEB and terminal ducts during puberty

To investigate whether BIM plays a role in postnatal mammary morphogenesis, whole-mount stained mammary glands dissected from $Bim^{-/-}$ female mice were examined (Bouillet et al., 2001). No significant differences between wild type and $Bim^{-/-}$ mammary glands were detected in glands from neonatal (1 week of age) or juvenile (3–4 weeks of age) periods of growth (see Figure S1). In addition, the overall pattern of ductal branching and expansion in the fat pad was indistinguishable in glands from wild type and $Bim^{-/-}$ mice throughout postnatal development (compare left panels of Figure. 2A, D, F to B, E, G and Figure S1). However, close examination of the TEBs from five weeks indicated that while wild type TEB contained a well-defined *lumen* (Figure 2A), the structures from $Bim^{-/-}$ mice were filled (Figure 2B). Quantification indicated that 86.6% ± 9.3 of the $Bim^{-/-}$ TEB lacked a detectable *lumen* at five weeks *versus* 4.4% ± 1.3 ($p<1E-04$) of the wild type TEB (Figure 2C). Analysis of the distribution of terminal end size revealed that 12.4% ± 3 of the $Bim^{-/-}$ distal structures were greater than 50000 μm^2 (terminal ends are designated as TEBs from 30000 μm^2 size range) compared to 5.5% ± 2.3 ($p<0.01$) in the wild type (Figure 2C). Thus, a significant percentage of the filled $Bim^{-/-}$ TEB displayed an increase in size. By six weeks, the distal ducts in the $Bim^{-/-}$ mammary gland that were filled at five weeks began to show marked hollowing; indicating that the ductal filling phenotype induced by loss of *Bim* was transient (Figure 2E). Finally, the $Bim^{-/-}$ ducts were completely hollowed at eight weeks and the whole mammary glands were indistinguishable from the wild type glands (compare Figure 2F to 2G).

Histological analysis of hematoxylin-eosin stained serial sections from wild type and $Bim^{-/-}$ mammary glands from five to eight weeks (Figure 3 and data not shown) confirmed the results of whole mount analysis described above (Figure 2). Although the TEB in wild type mice at

five weeks contained clearly discernable cap and body cells (Figure 3A) and the luminal and myoepithelial cell bilayer was organized in the ducts (Figure 3C), the luminal space in the *Bim*$^{-/-}$TEB (Figure 3B) and distal ducts (Figure 3D–F) was almost completely filled with epithelial cells. This inner cell population was composed of an unorganized epithelial mass (Figure 3B,E) and scattered structures that resemble squamous cell clusters (see Figure 3B,F). These data demonstrate that the loss of *Bim* perturbs the morphogenesis of TEBs and distal ducts and may lead to squamous transdifferentiation of a subset of the epithelial inner cell population. At six weeks, a similar mixture of epithelial and squamous cells was still detectable in the remaining filled ducts (Figure 3H). In addition, isolated squamous clusters embedded in a basophilic secretion (stained by eosin) were also observed in the hollowed proximal ducts of the *Bim*$^{-/-}$mammary glands (Figure 3I). Histological analysis of eight week-old *Bim*$^{-/-}$ mammary glands (Figure 3K–L) revealed differences with the wild type glands (Figure 3J) that were not detectable in the whole-mount staining (Figure 2F–G). At eight weeks, *Bim*$^{-/-}$ ducts were completely hollowed, but contained some acidophilic debris (stained by hematoxylin) encased in a basophilic secretion (Figure 3K and L), as well as ghost cells (cells with pale pink nucleus and transparent cytoplasm) (Figure 3L) in the proximal and distal ducts. The wild type mammary ducts contained a basophilic secretion with no evidence of acidophilic debris (Figure 3J). Interestingly, neither inflammation nor stromal activation was detectable by histology in the *Bim*$^{-/-}$ mammary gland at all the stages examined in this study (data not shown). Thus, these data indicate that the failure to clear a *lumen* in *Bim*$^{-/-}$ mammary glands is transient and also suggest that a death process independent of *Bim* can clear the mammary ducts.

The transient luminal filling observed in the *Bim*$^{-/-}$ mammary gland correlates with decreased apoptosis in the terminal end bud during puberty

Based on the pro-apoptotic function of *Bim*, we hypothesized that the lack of *lumen* formation observed in *Bim*$^{-/-}$ TEB and ducts at five weeks could be a consequence of decreased apoptosis of body cells. Using the TUNEL method to detect apoptotic cells, we found that the percentage of TUNEL positive cells in *Bim*$^{-/-}$ TEBs (1.1% ± 0.45) is dramatically reduced compared to wild type TEBs (10.6% ± 1.7, p<1E-04) (Figure 4A-B-E). Similarly, an antibody recognizing activated caspase 3 confirmed that apoptotic activity was decreased in the *Bim*$^{-/-}$TEBs (1.86% ± 0.38) compared to wild type counterparts (10.7% ± 1.75, p<1E-04) (Figure 4C to E). Although the pro-apoptotic function of BIM and other BH3-only proteins is well documented and it is therefore likely that the *Bim*$^{-/-}$ filling phenotype is largely explained by the loss of apoptosis in the TEBs and ducts, we investigated whether enhanced proliferation and/or altered cell differentiation could also contribute to the luminal filling. Quantification of BrdU incorporation revealed a slight decrease in the percent of proliferating TEB cells in *Bim*$^{-/-}$ TEBs compared to wild type TEBs (Figure 4F–H), most likely due to the increased number of TEB body cells. The proliferation rate of the cap cells in *Bim*$^{-/-}$ TEB (42.8% ± 6.6) was comparable to control TEBs (42.4% ± 5.4), while supernumerary cells in the center part of the filled *Bim*$^{-/-}$ TEBs did not incorporate BrdU (Figure 4G). To assess whether the loss of *Bim* affects the differentiation of TEB cells, we immunostained glands from 5-week-old mice with antibodies that recognize either the transcription factor p63 (basal cell marker) or MUC1 (luminal cell marker). Cap cells and scattered basal cells specifically expressed p63 while the luminal body cells were positive for MUC1 (Figure 4I). According to the analyzed markers (Figure 4I–J), loss of *Bim* does not appear to prevent cells from differentiating into expected cell subpopulations. Moreover, the expression patterns of luminal pubertal markers such as estrogen receptor alpha and progesterone receptor were not altered in the *Bim*$^{-/-}$ mammary epithelial bilayer (data not shown). Taken together, these data confirmed the conclusion that the inhibition of *lumen* development in the *Bim*$^{-/-}$ TEBs was due to a defect in apoptotic cell death.

The mammary cells in the clearing luminal space of the *Bim*$^{-/-}$ mammary glands undergo caspase-independent cell death at six to seven weeks

A careful analysis of the architecture of the *Bim*$^{-/-}$ glands revealed that ductal cells with epithelial morphology were separated from the outer luminal epithelial cells and organized into large isolated ductal islets (Figure 4K–O). The segregation of these islets could result from loss of adhesion to the outer luminal epithelial cells since E-cadherin is lost from the apical membrane of luminal cells after polarization. The integrity of cells in these clusters was also lost over time (see loss of β-catenin staining in Figure 4K–O) and TUNEL staining revealed detection of fragmented DNA (Figure 4K–L). Interestingly, there was very little evidence of apoptosis in these cell clusters based on the near absence of staining with antibody to activated caspase 3 (Figure 4M–O), cellular blebbing, or condensed nuclei (Figure 4K–O). The activation of caspase 3 (the terminal caspase in the pathway) was monitored as readout for activation of the caspase cascade since it is downstream of both intrinsic and extrinsic apoptotic pathways. However, in addition, we found that caspase 8 was not activated in the *Bim*$^{-/-}$ ducts at five or six weeks based on immunohistochemistal analysis (data not shown), and neither activated caspase-8 (Figure S2) nor truncated BID (tBID), a reporter of caspase 8 activity (data not shown), were detected by immunoblotting at the same stages. These results suggested that the centrally localized cells die by a caspase-independent cell death (CICD) mechanism. The squamous clusters in the filled ducts also displayed a similar CICD process at six to seven weeks (Figure 4P–Q). Quantitatively, we observed a 14.1-fold increase in the number of TUNEL positive cells (10.6%±0.8) compared to apoptotic cells with active caspase 3 (0.75% ±0.15 p<1E-04) in the filled duct at 6 weeks (see Figure 4R). As a control, equivalent amounts of caspase 3 activity and DNA fragmentation (TUNEL) were detected in the filled *Bim*$^{-/-}$ TEB, as reported above (see Figure 4E). Our findings suggest that caspase-independent death programs can occur in the *Bim*$^{-/-}$ mammary glands and clear the ductal luminal space with a delay of several weeks.

Detachment from matrix, growth factor withdrawal, and other events that compromise cellular metabolic activity can lead to elevated levels of reactive oxygen species (ROS) which can contribute to necrotic cell death, independent of apoptosis (Li et al., 1999). We therefore monitored ROS production to evaluate whether the non-apoptotic ductal cells in *Bim*$^{-/-}$ glands are subjected to oxidative stress. Lipid oxidation levels revealed by immunoreactivity of oxidative biomarkers, such as 4-Hydroxynonenal (4-HNE), are commonly used as a readout for reactive oxygen species ROS-induced stress (Boldogh et al., 2005). Interestingly, significant levels of 4-HNE were detected by immunohistochemistry in the compromised *Bim*$^{-/-}$ cell clusters (Figure S2), Furthermore, S100A7 (psoriasin), a calcium-binding protein, has been shown to be induced in response to ROS-mediated stress in mammary epithelium (Carlsson et al., 2005). In agreement with our finding of high levels of 4-HNE, induction of S100A7 was also observed by immunoblot in the *Bim*$^{-/-}$ mammary glands when compared to control glands (Figure S2). Thus, our data indicate that ROS-induced stress is detected in the absence of *Bim* and is likely to contribute to the CICD process identified in the *Bim*$^{-/-}$ mammary ducts.

Squamous differentiation in the filled *Bim*$^{-/-}$ TEB and distal ducts

As described above, our initial histological analysis revealed the presence of swirled arrays of cells that resembled squamous cell clusters in the *Bim*$^{-/-}$ TEBs and ducts. To better characterize these cell populations and provide clues to their lineage derivation and the mechanism associated with this abnormal differentiation, we first analyzed the expression of a variety of markers in the wild type and *Bim*$^{-/-}$ TEB. There was a 5.6 fold increase in the number of p63^{pos} cells in the *Bim*$^{-/-}$ TEB (32% ± 1.2, n=3) compared to the wild type TEB (5.7% ± 1.2, n=4) and the squamoid clusters were p63^{pos} (Figures 4J and S3) suggesting a basal cell origin. However, the absence of β1-integrin (β1-INT) (Figure 5B) and α smooth muscle actin (αSMA)

as well as the expression of keratin 6 (K6) (Figure S3) distinguished the p63^{pos} squamous clusters from the p63^{pos}αSMA^{pos}β1-INT^{pos} K6^{neg} scattered basal cells observed in the wild type TEB (see Figure 5K and Figure S3 for more details). The squamous clusters were also distinguished from basal body cells present in the *Bim*$^{-/-}$ TEB by their higher levels of cytoplasmic β-catenin and basal keratins such as keratin 14 (K14) (Figure 5D) and keratin 5 (K5) (data not shown). Interestingly, neither the p63 positive squamoid nor the basal body cells incorporated BrdU, indicating lack of proliferation in these cell populations (Figure 5F and Figure S3).

In the skin, squamous differentiation is also associated with loss of β1-integrin as well as contact with ECM proteins. Staining of filled *Bim*$^{-/-}$ TEBs with antiserum to Laminin (LN), demonstrated that cap cells as well as p63^{pos}β1-INT^{pos} basal body cells in wild type (Figure 5G) and *Bim*$^{-/-}$ TEBs (Figure 5H–J) expressed LN. However, a careful analysis by confocal microscopy showed that the basal body cells do not deposit LN (Figure 5G and I), whereas cap cells did (Figure 5J). A similar expression pattern was observed for collagen IV, another ECM protein (Figure S5). Furthermore, neither fibronectin nor fibrillar collagen expression was detected within wild type or *Bim*$^{-/-}$ TEBs (see Figure S5). Our data suggest that the cells in the filled TEB are deprived of ECM attachment.

The *Bim*$^{-/-}$ ducts contained similar cell populations to the TEB within the filled *lumen*. Inside of an outermost K8^{pos} MUC1^{pos} polarized luminal population, was a p63^{pos}β1-INT^{pos} inner basal cell population, and a p63^{pos}β1-INT^{neg} population of squamous cells (see Figure 6M). The non-squamous basal p63^{pos} MUC1^{neg}β1-INT^{pos} K5^{pos} sub-population was different from the p63^{pos}αSMA^{pos} LN^{pos}β1-INT^{pos} TEB basal cells. The inner basal cells in the ducts were not scattered, but localized in the most inner cell layer of the epithelial islets (Figure 6B–C) and did not express αSMA (Figure S4) or LN (Figure 4K–L). In the duct, the β1-INT^{neg} squamous clusters (Figure 6E–F) were distinguished by their organization into keratin pearls (foci with central keratinization surrounding concentric layers of abnormal squamous epithelial cell, see also Figures 3F and S4) and the expression of Keratin 10 (K10) (a specific marker of granular skin layer) (see Figure 6H–I). We did not detect expression of hair cortex cytokeratin, keratin 15 or CD34 (follicular lineage markers), suggesting that the *Bim*$^{-/-}$ mammary cells were undergoing an interfollicular squamous differentiation program (data not shown). The expression of p63 was concomitantly lost in the innermost cells of the ductal keratin pearls (Figure S4). However, we failed to detect expression of markers of terminal skin differentiation such as filaggrin, involucrin and loricrin (specific for cornified skin layer) (data not shown). Again, neither laminin (Figure 6K–L), collagen IV, nor fibronectin were detectable in the inner cell population (Figure S5). Thus, the loss of *Bim* triggered the development of interfollicular squamous cells that underwent a partial cornification process in the ducts.

Squamous transdifferentiation of mammary cells *in vitro* upon anoikis

Squamous differentiation in the *Bim*$^{-/-}$ mammary glands was an unexpected finding (see Figures 5, 6, S3 and S4). We propose that MECs, similar to their epidermal counterparts the keratinocytes, may undergo squamous differentiation when deprived of matrix attachment (Candi et al., 2005). We tested this hypothesis by analyzing the expression of squamous markers in two non-transformed MEC lines following detachment from ECM *in vitro*. Interestingly, both MCF10A and HMEC^{hTert} cells underwent squamous differentiation within 24 hours following loss of ECM attachment (Figure 7A). Under these conditions, the levels of skin differentiation markers such as K10 (specific of granular skin layer) and fillagrin (FIL, specific for cornified skin layer) were up-regulated in these cell lines. Immunofluorescent staining of cytospin preparations of MCF-10A cells suspended for 24 and 48 hours confirmed the up-regulation of K10 (Figure 7C and data not shown, quantified in Figure 7D) and FIL (Figure 7F and data not shown). In good agreement with our *in vivo* findings, MCF-10A cells

did not express hair cortex keratin, keratin 15 or CD34 upon suspension (data not shown). Previous reports showed that constitutive activation of the β-catenin pathway triggered squamous transdifferentiation of mammary epithelium (Miyoshi et al., 2002; Teuliere et al., 2005). In order to test a potential involvement of the β-catenin pathway in squamous transdifferentiation during anoikis of MCF-10A cells, we monitored β-catenin/TCF pathway activity in suspended MCF-10A cells. No significant difference in TCF activity (as assayed by TOPflash/FOPflash luciferase reporter ratio) was observed after 24h (1.3 ± 0.3, n=4) and 40h (2.4 ± 0.9, n=4) in suspension compared to attached MCF-10A control cells (1.7 ± 0.6, n=8). On the other hand, p38 mitogen-activated protein kinase (MAPK) activation was reported to promote interfollicular keratinocyte differentiation (Eckert et al., 2002). Unlike β-catenin/TCF pathway activity, p38 MAPK activity was up-regulated in MCF-10A cells upon anoikis (see figure 7G). Pharmaceutical inhibition of p38 MAPK activation with SB203580 (figure 7H) or SB202190 (data not shown) in MCF-10A cells prevented Keratin 10 (Figure 7H) and Keratin 1 (K1) (data not shown) up-regulation in suspension. Taken together, these results suggest that squamous differentiation of mammary cells upon anoikis, which occurred in the absence of a detectable increase in β-catenin activity, was p38 MAPK dependent.

We also tested whether MEC lines undergo squamous differentiation upon formation of spherical acini when cultured in reconstituted basement membrane. We hypothesized that the inner cell populations in 3D acini, like the inner cells in the $Bim^{-/-}$ ducts, might show squamous differentiation upon loss of matrix attachment. Although a squamous population of inner cells was not a common feature of MCF10A acini (data not shown), we found that $HMEC^{hTert}$ cells underwent dramatic squamous differentiation in 3D culture (Figure 7I). The $HMEC^{hTert}$ acini contained centrally localized squamous pearls that lacked β1-integrin and displayed stratified cells expressing K10 and K1 (also specific of granular skin layer) in the outermost layers and loricrin, (a marker for terminal skin differentiation) in the innermost layer (Figure 7J–K). Meanwhile, the outermost cell layer, which maintained contact with the ECM (Figure 7L), did not show evidence of skin differentiation, indicating that this process was likely induced by loss of ECM attachment. Taken together, these studies indicate that mammary epithelial cells undergo squamous differentiation when they are deprived of matrix.

Discussion

BIM regulates apoptosis during mammary ductal morphogenesis

The data presented here demonstrate that the BH3-only protein BIM plays a role in mammary ontogenesis in the mouse. BIM is required for the induction of apoptosis in the body cells of the developing TEB. The failure of $Bim^{-/-}$ TEB body cells to undergo apoptosis prevents *lumen* formation in TEBs and causes a delay in the clearing of adjacent ducts. Cells that fail to undergo apoptosis in ducts do eventually die by CICD.

Previously, Humphreys *et al.* showed that mammary TEBs displayed a striking pattern of apoptosis, restricted to an area near the presumptive luminal spaces. About 11% of the cells in the TEB appeared to undergo this death process at any given time by TUNEL staining (Humphreys et al., 1996). This led to the proposal that programmed cell death (PCD) in the highly proliferative TEBs maintains the *lumen* within the expanding duct. Moreover, this PCD process was previously shown to be independent of p53 and to be partially suppressed when the pro-survival protein BCL-2 was over-expressed (Humphreys et al., 1996). Neither the molecular mechanisms underlying the program that regulates death upstream of caspase activation nor the consequences of inhibition of apoptosis had been defined. Here, we show that the loss of *Bim* triggers an approximately 10-fold decrease in apoptotic cell death in the TEB (to 1.1%). Humphreys and colleagues described only an approximately 1.5 fold decrease (to 6.3%) due to the over-expression of *Bcl-2* under the control of the WAP promoter. In contrast to the phenotype reported for *WAP:Bcl-2* mice, we did not detect any dramatic

apoptotic activity in the neck of the filled *Bim*$^{-/-}$ TEBs, but rather a luminal filling in the distal ducts. Interestingly, hyper-activation of the Hedgehog signaling pathway in *Patched*$^{+/-}$ mice has also been reported to produce a transient distal luminal filling, however this effect is independent of any perturbation of cell apoptosis or proliferation rate (Lewis et al., 1999).

Remarkably, the process of *lumen* formation in MCF-10A 3D basement membrane cultures shares many features with clearance of excess cells in the TEBs and ducts during pubertal expansion. For instance, both processes involve BIM-dependent apoptosis. Inhibition of apoptosis delays, but does not prevent, the formation of a hollow *lumen* in both models (Debnath et al., 2002; Reginato et al., 2005). Thus, our *in vivo* data provide evidence for the relevance of 3D *in vitro* models for analysis of certain aspects of mammary morphogenesis.

Caspase-independent cell death in epithelial morphogenesis

Our data suggest that CICD can compensate for the loss of BIM-dependent apoptosis in the formation of a luminal space in mammary gland ducts during puberty. By definition, CICD occurs when there is a failure of apoptotic stimuli to activate caspases (Chipuk and Green, 2005). Usually this process is revealed *in vitro* after treatment with caspase inhibitors and *in vivo* when the pathway is genetically disrupted. In *Bim*$^{-/-}$ filled ducts at 6 weeks, the number of apoptotic cells is extremely low, yet TUNEL staining revealed the presence of DNA fragmentation within epithelial islets and squamous pearls, highlighting a CICD program. Even though the TUNEL assay is routinely used for examining apoptosis/PCD, this technique labels the 3′-OH termini of DNA breaks which are generated during both apoptosis and necrosis (Chipuk and Green, 2005). Indeed, these TUNEL positive cells in the *Bim*$^{-/-}$ ducts displayed necrotic features such as compromised cytoarchitecture and karyolysis, as well as evidence of oxidative stress (lipid oxidation and psoriasin expression), and lacked apoptotic features such as cellular blebbing and nuclear condensation. CICD has been observed in several mouse models in which apoptotic mediators are deleted by homologous recombination such as *Caspase 3*$^{-/-}$, *Caspase 9*$^{-/-}$ or *Apaf-1*$^{-/-}$ mouse models (Chipuk and Green, 2005). Caspase activation and apoptosis are ultimately not required for *lumen* formation of the mammary gland *in vivo*. Our study strongly suggests that CICD is an efficient backup mechanism to compensate for compromised apoptotic core machinery during epithelial ontogenesis.

Potential contribution of other BH3-only proteins in apoptotic cell death during mammary gland development

Although our data implicate a CICD process in the clearing of *Bim*$^{-/-}$ ducts, apoptotic cell death was not completely inhibited. We observed a small number of cells undergoing apoptotic PCD (0.75%) in the *Bim*$^{-/-}$ TEB and clearing *Bim*$^{-/-}$ mammary ducts, suggesting that other pro-apoptotic factors may act in parallel to BIM and/or compensate for *Bim* loss, albeit to a minor extent. We therefore cannot exclude the possibility that residual caspase-associated apoptosis participated in a minor way to the clearance process observed in the *Bim*$^{-/-}$ ducts. It remains to be determined which other BH3-only proteins, if any at all, could be responsible for the residual apoptosis in the *Bim*$^{-/-}$ mice. With the exception of BIM (this study), BAD is the only BH3-only protein whose expression has been thoroughly investigated in the mammary gland; however, BAD expression was not detectable during virgin development and was up-regulated only during lactation (Metcalfe et al., 1999). Regardless, any other putative pro-apoptotic factors that could have compensated for BIM loss in apoptotic cell death during mammary ductal morphogenesis may do so very poorly, as caspase-independent cell death appeared to be the main contributor to luminal clearing in the absence of *Bim*.

Squamous transdifferentiation of mammary epithelial cells

Squamous differentiation in the *Bim*$^{-/-}$ mammary glands was an unexpected finding. During skin differentiation, the lack of ECM attachment in keratinocytes leaving the basal layer,

concomitantly with the loss of β1-integrin expression, is known to initiate their differentiation (Candi et al., 2005). Here, we show for the first time that lack of ECM attachment may trigger a similar process in mammary cells.

In wild type TEBs, the main constituents of the body cell population are luminal cells and only a few scattered basal cells, however, the basal body cell population was amplified in the *Bim*$^{-/-}$ TEB. We speculate that the squamous cells are derived from this amplified but quiescent basal cell population deprived of ECM attachment because the squamous cells are positive for p63 and K5 and negative for the luminal markers K8 and MUC1. However, unlike basal body cells, the squamous cells are negative for β1-integrin, LN and αSMA, and positive for K10, a specific marker of the granular skin layer. The lose β1-integrin and LN expression in the mammary body cells correlated with squamous transdifferentiation; the same changes in gene expression accompany basal cell differentiation into squamous cells in the skin (Candi et al., 2005). The failure to detect markers of the cornified layer suggests that the skin differentiation program might not be carried out to completion. Also, CICD could eliminate these quiescent cells before their complete differentiation and thus prevent detection of these stratification markers.

Our *in vivo* observations in the *Bim*$^{-/-}$ mammary gland are reinforced by our *in vitro* study of non-transformed mammary cells, which display features of squamous differentiation upon detachment from matrix. Microarray analysis of MCF-10A cells in suspension (i.e. undergoing anoikis) has also revealed the existence of a transcriptional epidermis development program (TS and JSB personal communication). Furthermore, the keratin pearls formed by the HMEC^{hTert} cells in 3D culture on reconstituted basement membrane mimic the skin differentiation process. These data show that mammary cells can undergo complete keratinization, with a perfect stratification from the outermost layers expressing markers of the granular layer to the innermost cells expressing proteins specific of the cornified layer.

It has been reported that squamous differentiation in the mammary gland can be induced by activation of the β-catenin pathway. In previous studies, the over-expression of stabilized β-catenin in mammary luminal cells (Miyoshi et al., 2002) and myoepithelial cells (Teuliere et al., 2005) resulted in the development of squamous metaplasia expressing follicular epithelial lineage markers. In the present study, we discovered that lack of ECM attachment and subsequent activation of the p38 MAPK signaling pathway triggered squamous differentiation of mammary cells, apparently independent of a β-catenin activation. In addition, this alternate mechanism promoted an interfollicular differentiation program, revealed by the absence of expression of follicular markers.

The concept of epidermal transdifferentiation of mammary cells is also supported by the fact that skin and the mammary gland share the same embryonic origin in the ectoderm. Therefore, we propose that squamous differentiation could be an intrinsic property of mammary cells. Finally, cornification is considered to function as a cell death process (Candi et al., 2005) and may act in parallel to CICD and PCD to eliminate mammary cells in an anoikis-like process within the luminal space. These data raise interesting questions about CICD and squamous differentiation as tumour suppressive mechanisms in mammary cells during anoikis, as repopulation of the luminal space with cancer cells is a hallmark of early breast tumors.

Experimental Procedures

Mouse strains

All experiments with mice were performed according to the guidelines of the IACUC committee of Harvard Medical School. *Bim* $^{-/-}$ and *Bim*$^{+/-}$ mice and embryos were generated as previously described (Bouillet et al., 2001) and were in the C57BL/6 background. C57BL/

6 wild type littermates were used as control at different stages of mammary development. The number of *Bim*$^{-/-}$ female mice used in this study at the different stages were as follows: 1 week (n=3), 4 weeks (n=3), five weeks (n=9), six weeks (n=9), eight weeks (n=6).

Whole-mount mammary gland staining and histology

For whole-mount staining, either the third or fourth pair of mammary glands were spread on microscope slides and stained with carmine alum overnight as described previously (Teuliere et al., 2005). *LacZ* expression on whole-mount mammary glands and embryos was monitored by detecting β-galactosidase activity as described previously (White et al., 2004).

For histological analysis, mammary gland specimens were fixed in methacarn or 4% paraformaldehyde in PBS and dehydrated. Samples were embedded in paraffin, then cut (5 μm sections) at the Rodent Histopathology Service Facility (Harvard Medical School, Boston) and stained with Hematoxylin (Vector Lab) and Eosin (Sigma-Aldrich). All digital images of light and fluorescence microscopy were acquired with a TE 300 fluorescence microscope (Nikon).

BrdU incorporation and TUNEL assays

To assess cell proliferation, wild type (n=4) and mutant (n=5) mice were injected intraperitoneally with 0.25 mg 5-Bromo-2′-deoxyUridine (BrdU) per gram of body weight 2 hours prior to sacrifice. BrdU incorporation was detected on sections by immunohistochemistry followed by a light counterstaining with Hematoxylin. 1000–1500 nuclei per sample were counted. To detect apoptotic nuclei, paraffin-embedded sections from wild type (n=5) and mutant (n=6) were analyzed by TdT digoxygenin nick-end labeling with Apoptag Plus kit (Chemicon) following the manufacturers instructions.

Cell culture and cDNA constructs

MCF-10A MECs were obtained from the American Type Culture Collection (Manassas, VA) and cultured according to ATCC instructions. HMEC cells were purchased from Cambrex (East Rutherford, NJ) and cultured according to manufacturers protocol. The HMEC^{hTert} cell line was generated with retrovirus produced from the pBabe-hygro:hTert vector as described previously (Overholtzer et al., 2006). For morphogenesis assays, HMEC^{hTert} cells were resuspended in MEGM medium (Cambrex). Eight-well RS glass slides (BD Falcon) were coated with 50 μl of Growth Factor-reduced Matrigel (BD Biosciences) per well. 5,000 cells were plated per well in MEGM medium containing a final concentration of 2% Matrigel. MEGM medium containing 2% Matrigel was replaced every 4 days (Debnath et al., 2003).

Information on immunoblot assay, anoikis, cytospin preparation, immunohistochemistry and antibodies can be found in the supplemental experimental procedures.

Supplementary Material

Refer to Web version on PubMed Central for supplementary material.

Acknowledgments

We are grateful to Dr. Kenna Mills Shaw for establishing the *Bim*$^{-/-}$ mice at Harvard Medical School (HMS). In addition, we would also like to thank Dr. Marie-Ange Deugnier, Dr Marisa M. Faraldo, Dr Jayanta Debnath and Dr Amy Hall for helpful discussions, Rebecca Hillenbrand, Eugene Yim and Hubert Park for skilled technical assistance in the mouse facility, Dr. Florence Guibal for the cytospin preparation and luciferase reporter assays, Dr. Loling Song and the Nikon Imaging Center at HMS for confocal imaging. This work was supported by grants from the NIH/NCI CA105134 and CA080111 (JSB), NHMRC (Canberra; program #257502), the Leukemia and Lymphoma Society SCOR grant #7015 and NIH CA043540-18 and CA80188-6 (AS), FRM and The Susan G. Komen Breast Cancer

Foundation PDF29406 (AAM), the Swiss National Science Foundation PA00A-105094 (TS), The Charles and Sylvia Viertel Charitable Foundation (PB) and NCI institutional training grant T32CA09361 (MO).

References

Boldogh I, Bacsi A, Choudhury BK, Dharajiya N, Alam R, Hazra TK, Mitra S, Goldblum RM, Sur S. ROS generated by pollen NADPH oxidase provide a signal that augments antigen-induced allergic airway inflammation. J Clin Invest 2005;115:2169–2179. [PubMed: 16075057]

Bouillet P, Cory S, Zhang LC, Strasser A, Adams JM. Degenerative disorders caused by Bcl-2 deficiency prevented by loss of its BH3-only antagonist Bim. Dev Cell 2001;1:645–653. [PubMed: 11709185]

Candi E, Schmidt R, Melino G. The cornified envelope: a model of cell death in the skin. Nat Rev Mol Cell Biol 2005;6:328–340. [PubMed: 15803139]

Carlsson H, Yhr M, Petersson S, Collins N, Polyak K, Enerback C. Psoriasin (S100A7) and calgranulin-B (S100A9) induction is dependent on reactive oxygen species and is downregulated by Bcl-2 and antioxidants. Cancer Biol Ther 2005;4:998–1005. [PubMed: 16082188]

Chipuk JE, Green DR. Do inducers of apoptosis trigger caspase-independent cell death? Nat Rev Mol Cell Biol 2005;6:268–275. [PubMed: 15714200]

Daniel CW, Strickland P, Friedmann Y. Expression and functional role of E-and P-cadherins in mouse mammary ductal morphogenesis and growth. Dev Biol 1995;169:511–519. [PubMed: 7781895]

Debnath J, Mills KR, Collins NL, Reginato MJ, Muthuswamy SK, Brugge JS. The role of apoptosis in creating and maintaining luminal space within normal and oncogene-expressing mammary acini. Cell 2002;111:29–40. [PubMed: 12372298]

Debnath J, Muthuswamy SK, Brugge JS. Morphogenesis and oncogenesis of MCF-10A mammary epithelial acini grown in three-dimensional basement membrane cultures. Methods 2003;30:256–268. [PubMed: 12798140]

Eckert RL, Efimova T, Dashti SR, Balasubramanian S, Deucher A, Crish JF, Sturniolo M, Bone F. Keratinocyte survival, differentiation, and death: many roads lead to mitogen-activated protein kinase. J Investig Dermatol Symp Proc 2002;7:36–40.

Frisch SM, Francis H. Disruption of epithelial cell-matrix interactions induces apoptosis. J Cell Biol 1994;124:619–626. [PubMed: 8106557]

Huang DC, Strasser A. BH3-Only proteins-essential initiators of apoptotic cell death. Cell 2000;103:839–842. [PubMed: 11136969]

Humphreys RC, Krajewska M, Krnacik S, Jaeger R, Weiher H, Krajewski S, Reed JC, Rosen JM. Apoptosis in the terminal endbud of the murine mammary gland: a mechanism of ductal morphogenesis. Development 1996;122:4013–4022. [PubMed: 9012521]

Lewis MT, Ross S, Strickland PA, Sugnet CW, Jimenez E, Scott MP, Daniel CW. Defects in mouse mammary gland development caused by conditional haploinsufficiency of Patched-1. Development 1999;126:5181–5193. [PubMed: 10529434]

Li AE, Ito H, Rovira II, Kim KS, Takeda K, Yu ZY, Ferrans VJ, Finkel T. A role for reactive oxygen species in endothelial cell anoikis. Circ Res 1999;85:304–310. [PubMed: 10455058]

Metcalfe AD, Gilmore A, Klinowska T, Oliver J, Valentijn AJ, Brown R, Ross A, MacGregor G, Hickman JA, Streuli CH. Developmental regulation of Bcl-2 family protein expression in the involuting mammary gland. J Cell Sci 1999;112(Pt 11):1771–1783. [PubMed: 10318769]

Miyoshi K, Shillingford JM, Le Provost F, Gounari F, Bronson R, von Boehmer H, Taketo MM, Cardiff RD, Hennighausen L, Khazaie K. Activation of beta -catenin signaling in differentiated mammary secretory cells induces transdifferentiation into epidermis and squamous metaplasias. Proc Natl Acad Sci U S A 2002;99:219–224. [PubMed: 11773619]

O'Reilly LA, Cullen L, Visvader J, Lindeman GJ, Print C, Bath ML, Huang DC, Strasser A. The proapoptotic BH3-only protein bim is expressed in hematopoietic, epithelial, neuronal, and germ cells. Am J Pathol 2000;157:449–461. [PubMed: 10934149]

Overholtzer M, Zhang J, Smolen GA, Muir B, Li W, Sgroi DC, Deng CX, Brugge JS, Haber DA. Transforming properties of YAP, a candidate oncogene on the chromosome 11q22 amplicon. Proc Natl Acad Sci U S A 2006;103:12405–12410. [PubMed: 16894141]

Reginato MJ, Mills KR, Becker EB, Lynch DK, Bonni A, Muthuswamy SK, Brugge JS. Bim regulation of lumen formation in cultured mammary epithelial acini is targeted by oncogenes. Mol Cell Biol 2005;25:4591–4601. [PubMed: 15899862]

Reginato MJ, Mills KR, Paulus JK, Lynch DK, Sgroi DC, Debnath J, Muthuswamy SK, Brugge JS. Integrins and EGFR coordinately regulate the pro-apoptotic protein Bim to prevent anoikis. Nat Cell Biol 2003;5:733–740. [PubMed: 12844146]

Teuliere J, Faraldo MM, Deugnier MA, Shtutman M, Ben-Ze'ev A, Thiery JP, Glukhova MA. Targeted activation of beta-catenin signaling in basal mammary epithelial cells affects mammary development and leads to hyperplasia. Development 2005;132:267–277. [PubMed: 15590737]

Wang P, Gilmore AP, Streuli CH. Bim is an apoptosis sensor that responds to loss of survival signals delivered by epidermal growth factor but not those provided by integrins. J Biol Chem 2004;279:41280–41285. [PubMed: 15292207]

White DE, Kurpios NA, Zuo D, Hassell JA, Blaess S, Mueller U, Muller WJ. Targeted disruption of beta1-integrin in a transgenic mouse model of human breast cancer reveals an essential role in mammary tumor induction. Cancer Cell 2004;6:159–170. [PubMed: 15324699]

Williams JM, Daniel CW. Mammary ductal elongation: differentiation of myoepithelium and basal lamina during branching morphogenesis. Dev Biol 1983;97:274–290. [PubMed: 6852366]

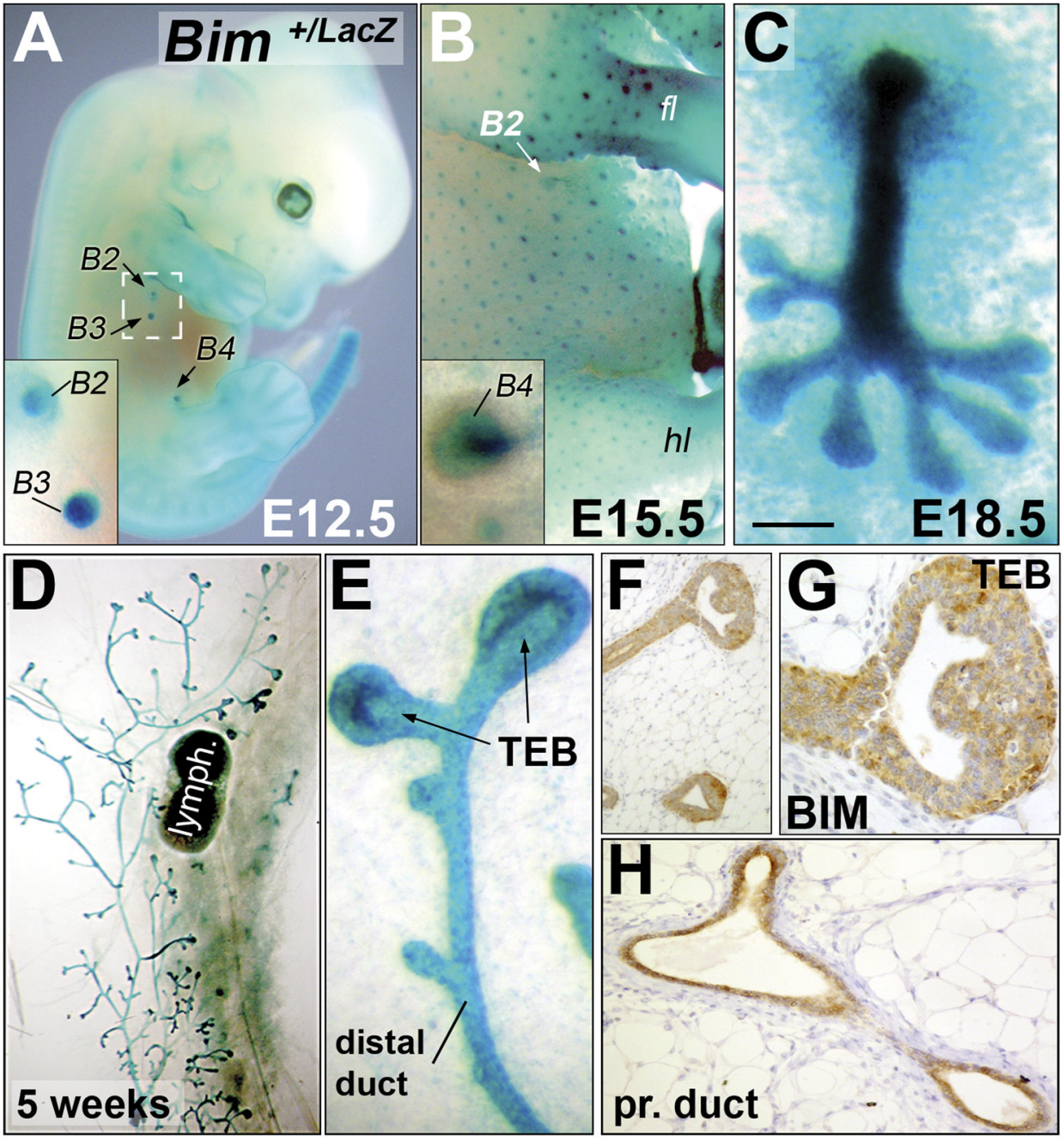

Figure 1. *Bim* expression in the developing mouse mammary gland

(**A**) X-gal stained E12.5 heterozygous *Bim*$^{+/LacZ}$ embryo. The **insert** shows a high magnification of the second and third pair of mammary buds. (**B**) X-gal stained E15.5 *Bim*$^{+/-}$ female embryo. *Bim* is expressed in the mammary and hair follicle buds. The **insert** shows a high magnification of a mammary bud (fourth pair). (**C**) X-Gal stained E18.5 *Bim*$^{+/-}$ female skin explant showing *Bim* expression in the mammary gland. (**D**) X-Gal staining of *Bim*$^{+/-}$ mammary gland at five weeks. (**E**) High magnification of a TEB and distal duct shown in D. (**F–H**) BIM immunostaining (Epitomics antibody #1036-1) of a TEB (F–G) and proximal duct (H) at five weeks. (**G**) High magnification of a TEB shown in F. [Scale bar: 1100 (A), 700 (B), 200 (A and B inserts, D), 100 (C), 20 (E,H), 25 (F), 12 (G) μm] *Abbreviation:*

fl (forelimb), hl (hindlimb), B# (mammary bud), lymph. (lymph node), TEB (terminal end bud), pr. (proximal).

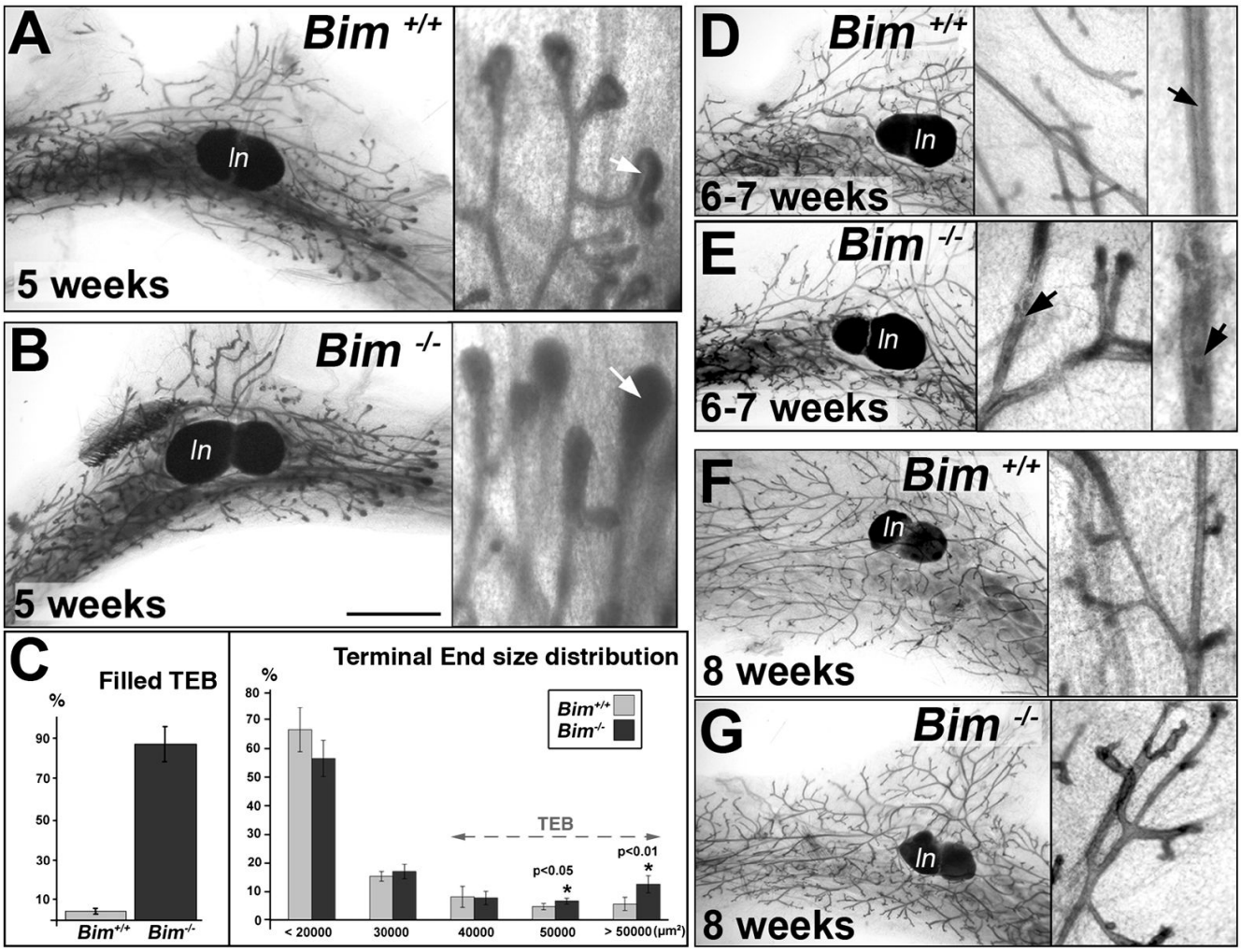

Figure 2. Comparison of whole mount *Bim*$^{-/-}$ and control mammary glands during puberty

(**A–B**) Whole mount staining of mammary glands from five week-old *Bim*$^{+/+}$ (A) and *Bim*$^{-/-}$ (B) mice at low (left panel) and high (right panel) magnification. The luminal space is filled (white arrow) in the *Bim* $^{-/-}$ TEB (B, right panel). (**C**) Morphometric study of *Bim*$^{-/-}$ TEB at five weeks. **Left panel**: percentage of TEB without any detectable luminal space in *Bim*$^{+/+}$ (4.4 % ± 1.3; n=7) and *Bim*$^{-/-}$ (86.6 % ± 9.3; n=8) mammary glands at five weeks. **Right panel**: size distribution (μm^2) of terminal ends of the ducts in *Bim*$^{+/+}$ (n=4) and *Bim*$^{-/-}$ (n=4) mammary glands at five weeks. The size distribution of terminal ends in the *Bim*$^{+/+}$ and *Bim*$^{-/-}$ glands is: 66.7%± 7.8 (+/+) and 56.6% ± 6.3 (−/−) for sizes below 20000 μm^2, 15.2% ± 1.7 (+/+) and 16.9% ± 2.6 (−/−) between 20000 and 30000 μm^2, 8% ± 3.7 (+/+) and 7.6% ± 2.3 (−/−) from 30000 to 40000 μm^2; 4.6% ± 1.1 (+/+) and 6.5% ± 1 (+/+) between 40000 and 50000 μm^2 (paired t-test with $p<0.05$); 5.5% ± 2.3 (+/+) and 12.4% ± 3 (−/−) for TEBs above 50000 μm^2 (paired t-test with $p<0.01$) (**D–E**) Whole mount staining of mammary glands from 6 to 7 week-old wild type (D) and *Bim*$^{-/-}$ mice (E) at low and high magnification. Note that the luminal space is clearing (black arrow) in E. (**F–G**) Whole mount staining of eight week-old wild type control (F) and *Bim*$^{-/-}$ (G) mammary glands at low and high magnification. [Scale bar: 300 (A-B-D-E), 450 (D–E), 550 (F–G), 60 (A-B-D-E-F-G insert), 30 (D–E right inserts) μm]. *Abbreviation: TEB (terminal end bud), ln (lymph node).*

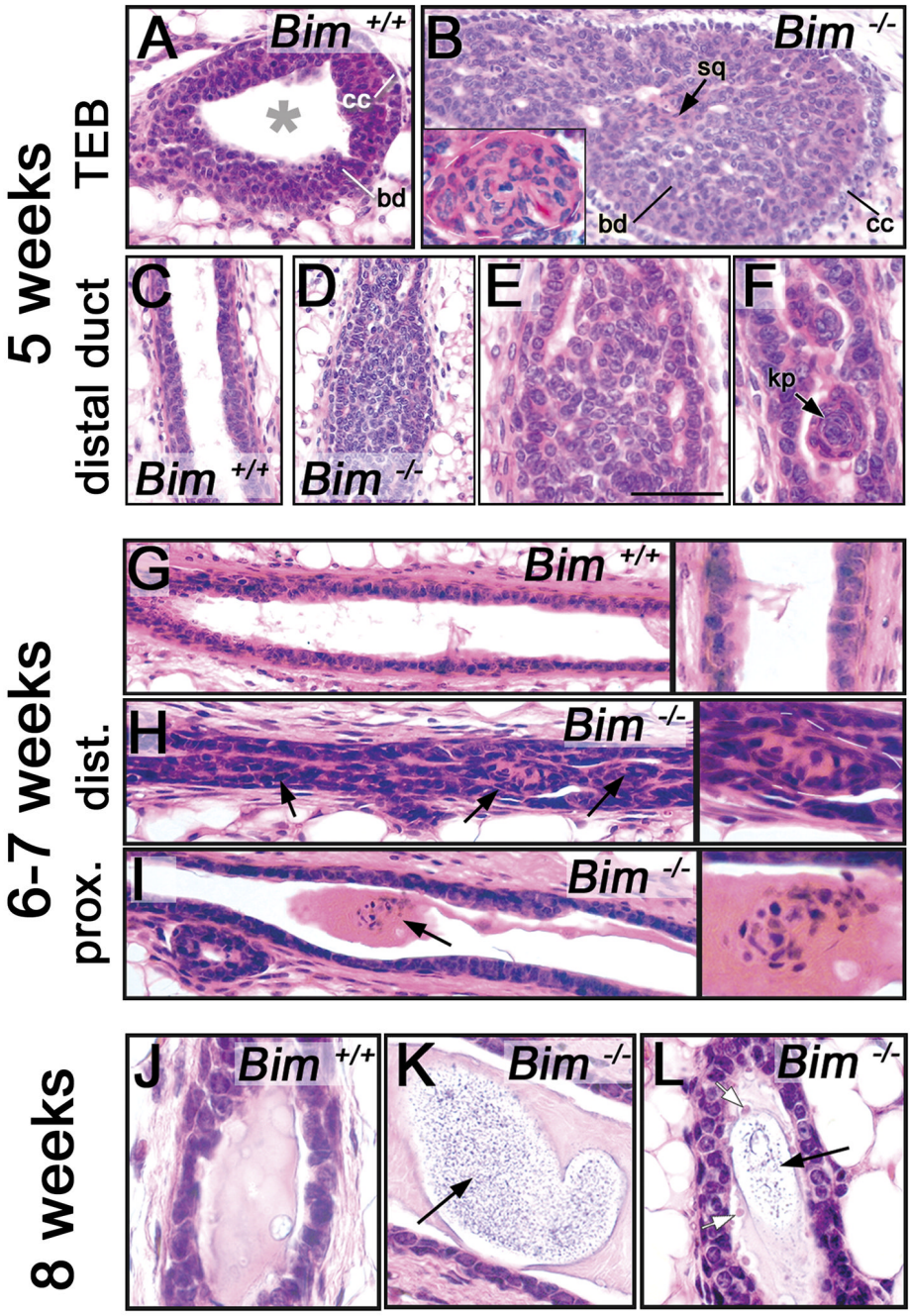

Figure 3. Histology of *Bim*$^{-/-}$ and control mammary glands from five to eight weeks

(**A–B**) Sections of a wild type hollowed TEB (A) and a filled *Bim*$^{-/-}$ TEB (B) at five weeks. (**B**) The **insert in B** shows a high magnification of a squamous cell cluster. (**C–F**) Sections of a wild type hollowed control mammary duct (C) and filled *Bim*$^{-/-}$ duct (D–F) at five weeks. (**E**) High magnification of the filled *lumen* shown in D. (**F**) High magnification of a scattered keratin pearl (black arrow) in a *Bim*$^{-/-}$ filled duct. **(G)** Section of a wild type hollowed mammary duct at six to seven weeks. **Right panel**: high magnification of G. (**H**) Section of a *Bim*$^{-/-}$ filled distal mammary duct at six to seven weeks. Note the cells filling the luminal space (black arrows). **Right panel**: high magnification of H. (**I**) Section of a *Bim*$^{-/-}$ proximal mammary duct at six weeks. Note the squamous cell cluster embedded in secretion (black

arrow). **Right panel**: high magnification of I. (**J**) Section of control mammary duct at 8 weeks. Note the presence of secretion in the luminal space. **(K)** Section of a hollowed *Bim*$^{-/-}$ proximal mammary duct at eight weeks with debris embedded in secretion (black arrow). **(L)** Section of a hollowed *Bim*$^{-/-}$ distal mammary duct at 8 weeks with ghost cells (white arrow) and debris (black arrow). [Scale bar: 10 (A–B), 3.5 (B insert), 50 (C–D), 20 (G-H-I), 6 (E-F-J-K-L, panels in G-H-I) μm]. *Abbreviation: cc (cap cell), bd (body cell), sq (squamous); kp (keratin pearl).*

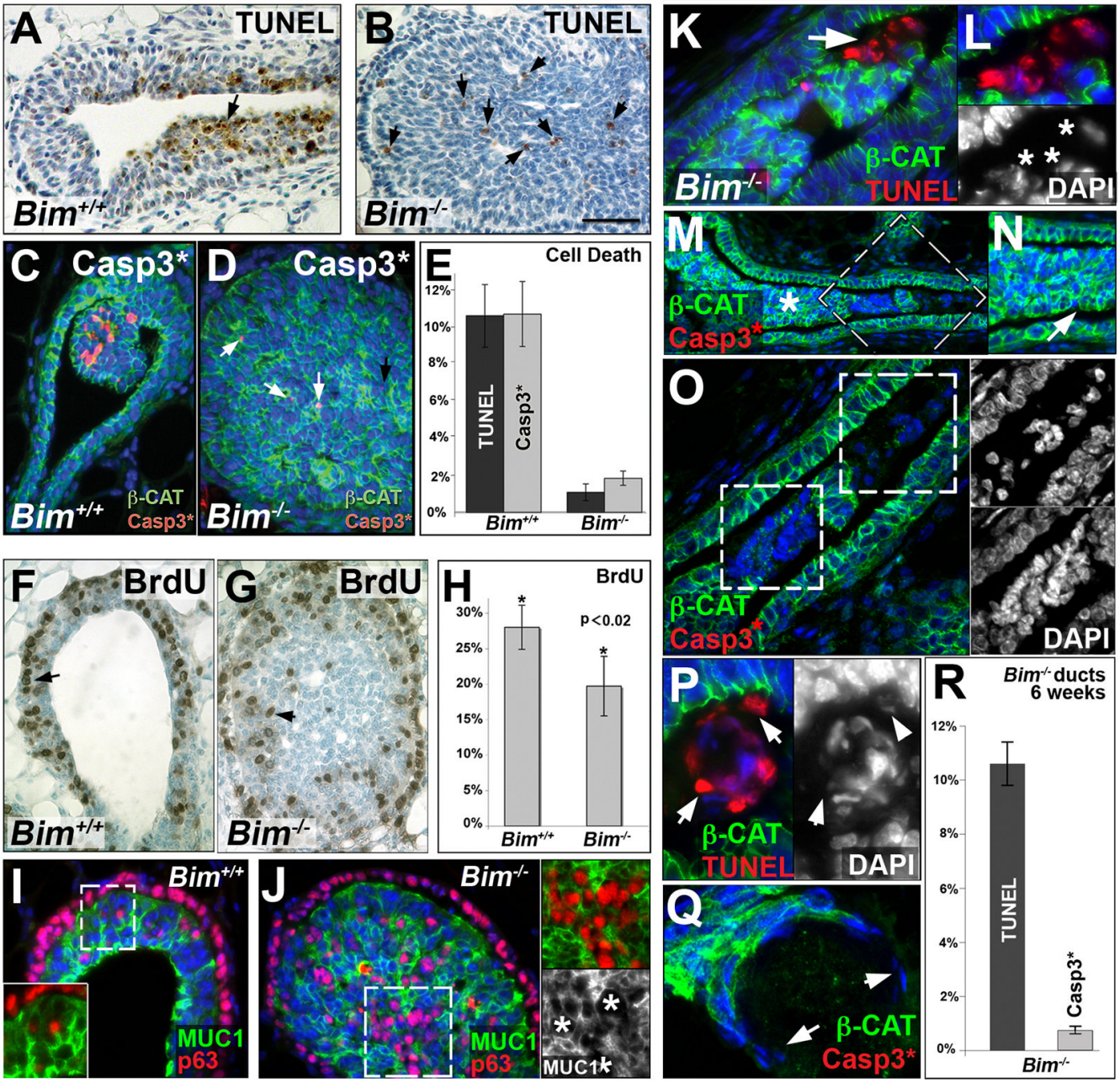

Figure 4. Cell death, proliferation and cell differentiation at 5 weeks and caspase-independent cell death at six weeks in *Bim*$^{-/-}$ mammary glands

(**A–B**) TUNEL staining of representative wild type TEB (A) and *Bim* $^{-/-}$ TEB (B) at five weeks. (**B**) Residual TUNEL staining (black arrows) is observed in *Bim*$^{-/-}$ TEB at five weeks. (**C–D**) Immunostaining of cleaved (i.e. activated) caspase 3 (red) and β-catenin (green) in a representative wild type TEB (C) and *Bim*$^{-/-}$ TEB (D) at five weeks. (**D**) Small numbers of cleaved caspase 3 positive cells (white arrows) are observed in *Bim*$^{-/-}$ TEB at five weeks. (**E**) Quantification of TUNEL and cleaved caspase 3 positive cells expressed as mean ± SD in the TEB of five week old mice (n=5 per genotype). Percentages of TUNEL positive cells were 10.6% ± 1.7 in wild type and 1.1% ± 0.45 in *Bim*$^{-/-}$ TEBs. Percentage of cleaved caspase 3 positive cells were 10.7% ± 1.75 in wild type and 1.86% ± 0.38 in *Bim*$^{-/-}$ TEBs. (**F–G**) BrdU

staining (black arrow) of representative wild type TEB (F) and a *Bim*$^{-/-}$ TEB (G) at five weeks. (**H**) Proliferation assay in TEB from five week-old mice (n=5 per genotype). The percentages of BrdU-positive cells were 28% ± 3.1 in wild type and 19.7% ± 4.2 in *Bim*$^{-/-}$ TEB (paired t-test with p<0.02). (**I–J**) MUC1 (green) and p63 (red) expression in wild type (I) and *Bim*$^{-/-}$ TEB (J). The **insert in I** shows a high magnification of MUC1 and p63 overlay from the dashed box. The **upper insert in J** shows a high magnification of MUC1 and p63 overlay from the dashed box. The **lower insert in J** shows MUC1 staining alone. Note that the p63 positive cells were MUC1 negative in the *Bim*$^{-/-}$ TEB (white asterisks). (**K–L**) Colocalization of β-CAT (green) and TUNEL (red) positive cells (white arrows) in *Bim*$^{-/-}$ clearing duct at 6 weeks by immunostaining. (**L**) High magnification of the cell cluster shown in K. **Lower insert**: corresponding DAPI staining (white asterisks). (**M–O**) Immunostaining of β-CAT (green) and cleaved caspase 3 (red) in filled *Bim*$^{-/-}$duct at six weeks. (**N**) High magnification of the area labeled with a white asterisk in M. Note that luminal epithelial cells are organized into large isolated ductal islets (white arrow). (**O**) High magnification of dashed box in M. **Upper and lower inserts** show corresponding DAPI staining of dashed boxes in O. (**P**) Immunostaining of β-CAT (green) and TUNEL (red) positive cells in a keratin pearl with TUNEL-positive cells (white arrows). **Right panel**: DAPI staining of the main panel. **(Q**) Immunostaining of β-CAT (green) and cleaved caspase 3 (red) in compromised squamous cluster in *Bim*$^{-/-}$ duct at six weeks. Note the absence of β-CAT staining and the thin shape of nuclei in the peripheral cells (white arrows). (**R**) Quantification of TUNEL-positive (10.6 ± 0.8%, n=3) and cleaved Casp3 positive (0.75 ± 0.15%, n=4) cells in the ducts of six week old *Bim*$^{-/-}$ mice. Nuclei are in blue. [Scale bar: 6 (A, B, C, D, F, G, N), 8 (I, J), 4 (K, P, Q, insert in J), 12 (M), 2.5 (L, O) μm]. *Abbreviation: β-Cat (β-catenin), Casp3* (cleaved caspase 3), MUC1 (Mucin-1).*

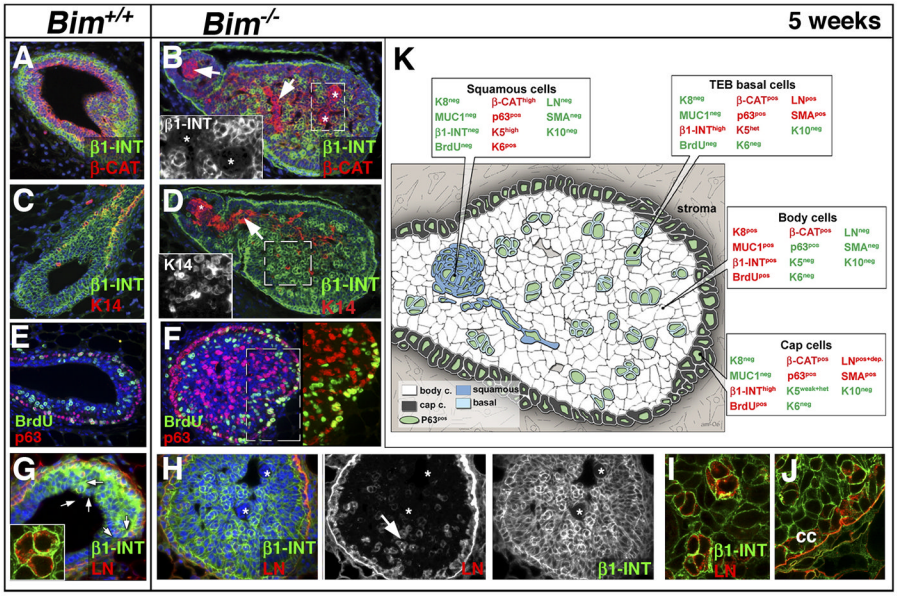

Figure 5. Characterization of the inner cell population of the filled *Bim*$^{-/-}$ TEBs at five weeks

(**A–B**) Colocalization by immunostaining of β1-INT (green) and β-CAT (red) in a wild type (A) and a *Bim*$^{-/-}$ (B) TEB at five weeks. (**B**) Note that the highly positive β-CAT clusters are β1-INT-negative (white arrows and asterisks). The **insert** shows a high magnification of the β1-INT-negative clusters in dashed box **(C–D)** Immunostaining of β1-INT (green) and K14 (red) in a wild type (C) and a *Bim*$^{-/-}$ TEB (D) at five weeks. Nuclei are in blue. (**D**) The β1-INT negative cell clusters in the TEB express high levels of K14 (white arrow). The **insert** shows that β1-INT^{pos} basal cells express K14 as well (dashed box in D). (**E–F**) BrdU incorporation (green) and p63 expression (red) in wild type (E) and *Bim*$^{-/-}$ TEB (F). **Right panel in F**: p63 and BrdU overlay of the dashed boxes shown in F. Note that the p63^{pos} cells in the TEB body did not incorporate BrdU. (**G–I**) Immunostaining of β1-INT (green) and LN (red) in a wild type TEB (G) and *Bim*$^{-/-}$TEB (H) at five weeks. (**G**) The insert shows cytoplasmic localization of LN in TEB basal cells (white arrows in G). (**H**) The β1-INT-negative cell clusters do not express LN (white asterisk). (**I**) Confocal imaging of basal cells in the TEB (see white arrow in H) showing a cytoplasmic localization of LN. (**J**) Confocal imaging of cap cells showing extracellular localization of LN. (**K**) Diagram summarizing the expression of differentiation markers in the cell populations present in a filled TEB at five weeks. Expressed proteins are in red and those not expressed in green. [Scale bar: 15 (A to H), 3 (I–J and G insert), 8 (A-B-D-F inserts) μm]. *Abbreviation: β1-INT (β1-integrin), β-Cat (β-catenin), LN (Laminin), K14 (keratin 14), cc (cap cells), BrdU (Bromodeoxyuridine).*

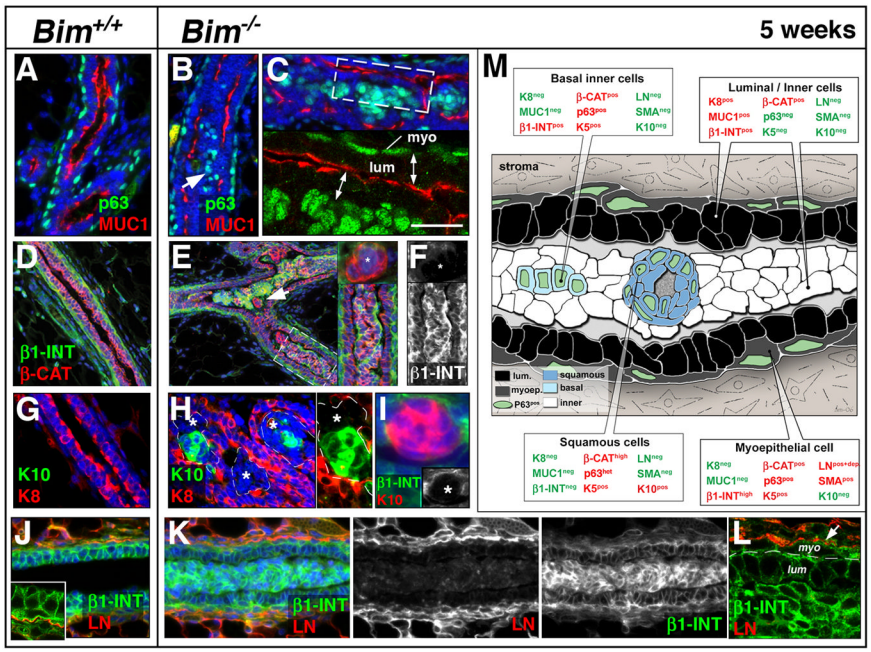

Figure 6. Characterization of the inner cell population of the filled *Bim*$^{-/-}$ ducts at five weeks

(A–C) Colocalization by immunostaining of p63 (green) and MUC-1 (red) in wild type (A) and *Bim*$^{-/-}$ (B–C) ducts (**A**) Note the apical localization of MUC-1 in luminal cells of the control duct while p63 expression is restricted to the myoepithelial cells. (**B–C**) Note that in the *Bim*$^{-/-}$ filled duct inner MUC1^{neg} cells express p63 (white arrow). The **lower panel in C** shows confocal imaging of dashed box shown in the upper panel. Note the apical localization of MUC1 in the luminal/inner cells (double head white arrows). **(D–F)** Immunostaining of β1-INT (green) and βCAT (red) in a wild type hollowed duct (D) and *Bim*$^{-/-}$ filled TEB **(**E–F). The **top insert in E** shows a β1-INT$^{neg.}$ squamous cluster (white arrow). The **lower insert in E** shows a high magnification of the dashed box. (**F**) Corresponding β1-INT staining of right insert in E. Note that the squamous clusters are β1-INT-negative (white asterisks). (**G–H**) Indirect immunofluorescence for K10 (green) and K8 (red) in *Bim*$^{+/+}$ (G) and *Bim*$^{-/-}$ (H) mammary ducts. (**H**) Note that only a subset of the K8-negative cells (white asterisks) are K10-positive. **Right insert** shows a high magnification of the left insert without DAPI staining. (**I**) Immunostaining of β1-INT (green) and K10 (red) of a keratin pearl in a filled distal *Bim*$^{-/-}$ *duct.* **Lower insert**: note that the keratin pearl is β1-INT^{neg}. (**J–L**) Immunostaining of β1-INT (green) and LN (red) in a wild type (J) and *Bim*$^{-/-}$distal duct (K–L). The **insert in J**: confocal imaging showing extracellular localization of LN in the mammary ducts. (**L**) Confocal imaging showing extracellular localization of LN at the level of the myoepithelial cells in the filled mammary ducts. (**M**) Diagram summarizing the expression of differentiation markers in the cell populations present in a filled *Bim*$^{-/-}$ distal duct at five weeks. Expressed proteins are in red and those not expressed are in green. [Scale bar: 15 (D-E-G-H-J-K), 10 (F, insert in E), 7 (A-B-C and insert in I), 3 (L and C–J inserts), 5.5 (H inserts) μm]. *Abbreviation: myo (myoepithelial cells), lum (luminal cell), β1-INT (β1-integrin), β-Cat (β-catenin), LN (Laminin), MUC1 (Mucin-1), K8 (keratin 8), K10 (keratin10).*

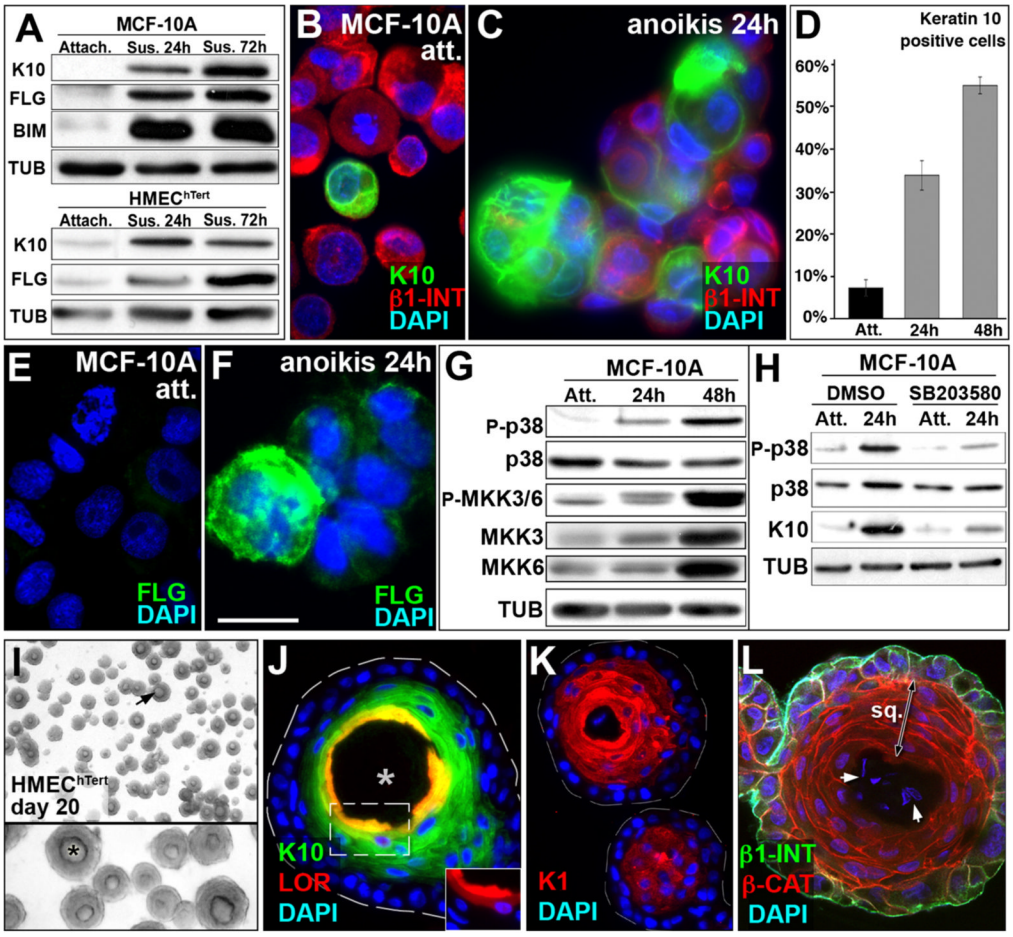

Figure 7. Squamous transdifferentiation of mammary epithelial cell lines *in vitro*

(A) Immunoblot showing K10 and FLG expression in attached cells and induction upon suspension at 24h and 72h in MCF-10A and HMEC^{hTert} cells. Note induction of BIM (Stressgen antibody AAP-330) in MCF-10A cells upon anoikis as described previously (Reginato et al., 2003). TUB was used as loading control. (**B–C**) K10 (green) and β1-INT (red) immunofluorescence on cytospin samples of attached cells (B) and cells in suspension for 24h (C). (**D**) Quantification of Keratin 10-positive MCF-10A cells for attached (7.24% ± 1.99) condition and after 24h (33.8% ± 3.46) or 48h (55% ± 2, $p<0.001$) in suspension. (**E–F**) FLG immunofluorescence on cytospin samples of attached cells (E) and cells in suspension for 24h (F). (**G**) Up-regulation of p38 MAPK pathway activity upon anoikis. Immunoblot showing up-regulation of phosphorylation of p38 MAPK and its upstream MAPKs, MKK3 and MKK6, upon suspension at 24h and 48h in MCF10A cells. Note that total level of MKK3 and MKK6 increased upon anoikis, while p38 MAPK protein did not change. TUB was used as a loading control. (**H**) Pharmacological inhibition of p38 MAPK activation suppressed K10 expression. SB203580 treatment (10μM in DMSO) decreased phosphorylation of p38 MAPK and prevented K10 up-regulation in suspension at 24h, while treatment with the carrier alone (DMSO) did not inhibit up-regulation of p38 MAPK phosphorylation and K10 protein expression. Note that total level of p38 MAPK protein does not change upon anoikis. TUB was used as a loading control. (**I**) Microphotography of HMEC^{hTert} acini after 20 days of culture. Note the "onion skin" shape of the inner cells (black arrow in low magnification panel). **Lower panel**: high magnification of the upper panel. Note the *lumen* (black asterisk). (**J**) Immunostaining for K10 (green) and LOR (red) in HMEC^{hTert} acini with a hollow *lumen* (white

asterisk) at day 20. The dashed white line displays $HMEC^{hTert}$ acinus borders. **Insert**: LOR staining alone with DAPI of the dashed box shown in the main panel. (**K**) Immunolocalization of K1 in $HMEC^{hTert}$ acini at day 20. (**L**) Colocalization of β1-INT (green) and β-CAT (red) by immunostaining in $HMEC^{hTert}$ acini at day 20. Note the absence of β1-INT expression in the squamous inner cells (double head arrow) and the faint DAPI staining in the center of the acinus (white arrows). [Scale bar: 15 (B-C-E-F), 430 (I), 180 (I insert), 35 (J–K), 45 (L) μm]. *Abbreviation: att. and Attach. (attached), ano. (anoikis), sus. (suspension), sq. (squamous), β1-INT (β1-integrin), β-Cat (β-catenin), FLG (Filaggrin), LOR Lloricrin), K1 (keratin 1), K10 (keratin 10), P-MMK3/6 (phospho-MKK3/6), P-p38 (Phospho-p38 MAPK), TUB (tubulin).*